UKRAINIAN CATHOLIC UNIVERSITY

MASTER THESIS

Corner localization and camera calibration from imaged lattices

Author:
Andrii STADNIK

Supervisor:
Dr. James PRITTS

A thesis submitted in fulfillment of the requirements for the degree of Master of Science

in the

Department of Computer Sciences
Faculty of Applied Sciences

Lviv 2022

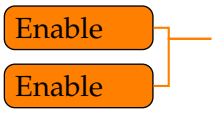
Enable
Enable

UKRAINIAN CATHOLIC UNIVERSITY

Faculty of Applied Sciences

Master of Science

Corner localization and camera calibration from imaged lattices

by Andrii STADNIK

Abstract

The Thesis Abstract is written here (and usually kept to just this page). The page is kept centered vertically so can expand into the blank space above the title too...

Camera calibration is a crucial step in many computer vision applications. Typically, it involves taking a set of images of a calibration pattern, detecting its' features, and estimating the camera parameters. However, under certain conditions (including occlusions, bad lightning, highly distorted images etc.), feature detectors might fail to detect some of the features..

In this paper, we propose a novel approach to feature detection in the context of camera calibration. After the initial feature detection and calibration, we use the intermediate camera parameters to predict the possible positions of the previously undetected features. Those features are filtered using the binary classifier, and the remaining features are used to further constrain the camera calibration.

Do I have to justify it?

Enable

Enable

Enable

Enable

Todo list

1 Remove list of todos

1. Introduction and motivation
   (a) Outline of the problem
   (b) Research objective
      - Finding new features by projecting the board
      - Robustly classifying the true and false positives
   (c) Thesis structure
2. Related work
   (a) Camera calibration
   (b) Calibration boards
   (c) Feature detection on calibration boards
   (d) Camera models
   (e) Camera parameters estimation
   (f) Search of the previously undetected features
3. Background
   (a) Notation
   (b) Camera model
      - Distortion model, inverse distortion model
      - Projection
      - Backprojection
   (c) Feature detection
   (d) Camera calibration (Probably I could move it to the Approach)
4. Approach
   (a) Feature detection
   (b) Camera calibration
   (c) Board projection, features classification
5. Experiments
   (a) Synthesizer
   (b) Datasets
   (c) Metrics
   (d) Results
6. Conclusions

I'll have to merge some-thing to have 5 chapters

Chapter 1

Introduction and motivation

1.1 Outline of the problem

Better camera calibration improves the performance of various downstream tasks by providing a more accurate mapping between 3D world coordinates and 2D image plane coordinates. This improved mapping enables precise alignment, positioning, and scaling of objects within the scene. By determining the camera's intrinsic and extrinsic parameters, algorithms can correct for lens distortion, estimate depth information, and accurately overlay virtual content. Consequently, tasks such as 3D reconstruction, augmented reality, and object detection can achieve better results in terms of precision, spatial consistency, and overall visual quality.

Although manufacturers can estimate camera calibration parameters a priori, fully automatic calibration is often preferred, especially when camera metadata is unavailable. Currently, wide-angle lenses, particularly in mobile phones and GoPro-type cameras, dominate consumer photography. These cameras pose additional challenges due to their requirement for highly non-linear models with numerous parameters. The high distortion of the image plane also makes finding key points robustly challenging.

Typically, camera calibration is obtained by capturing an image of a known calibration pattern, which is then used to estimate the camera parameters. Alternatively, some methods do not use a calibration pattern but instead infer geometric constraints directly from the scene. However, this approach is generally less accurate.

As reported by Duisterhof et al. (2022) on Oct. 5, 2022, the current state-of-the-art methods (**olsonAprilTagRobustFlexible2011a**; Schöps et al., 2020; Krogius, Haggenmiller, and Olson, 2019) fail on images with high distortion. Duisterhof et al., 2022 suggested an iterative the approach of image undistortion and target reprojection, achieving the superior robustness to the noise than the state-of-the-art methods because the feature detection is performed on the undistorted image.

Instead of searching for the features on the undistorted image from scratch, it is possible to utilize the prior knowledge of the geometry of the calibration board, effectively predicting the possible positions of previously undetected features. It can be done by projecting the board onto the image using the intermediate camera calibration, and then filtering the possible positions in order to eliminate false positives.

This additional points will further constrain the camera calibration, improving the accuracy of the calibration parameters.

Explain why more features is better

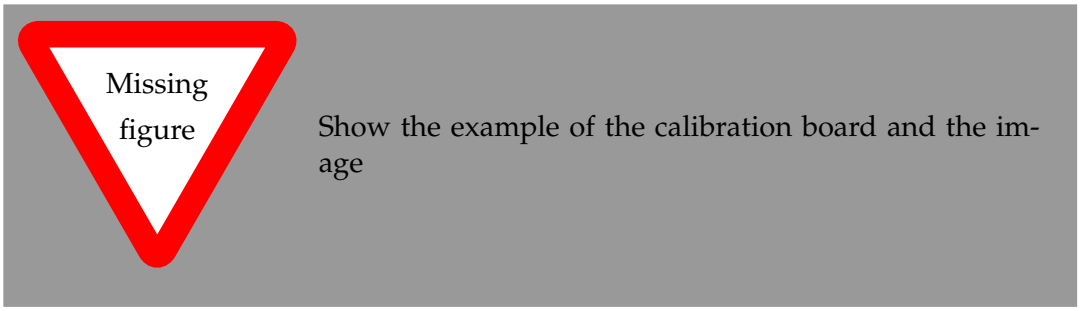

1.2 Research objective

The objective of this research is to improve the accuracy of the camera calibration by finding previously undetected features on the calibration board . For that, we formulate the set of research questions:

- How to find additional features on the calibration board which were not detected by the feature detector?
- How to filter out falsely detected features?

Probably rephrase if I won't compare the actual calibration

Add more

1.3 Thesis structure

This paper has the following structure: in **??**, we will describe the related work, including the literature search method and methodology, various subtopics of the camera calibration, mention conjugate translations, and outline the state-of-the-art solutions. We define the research gap in **??** and outline the proposed approach to solution and evaluation in **??**. We will describe the early results in **??**, including the dataset analysis, feature detector, and conjugately translated points simulator. In **??**, we will summarize the results and outline future work.

Update

Chapter 2

Related work

2.1 Camera calibration

Getting the correspondence between the spatial and the image coordinates requires camera calibration. Camera calibration consists of the geometric camera model and the parameters of this model. That information makes it possible to obtain the 2d image coordinates of any point in the 3d space.

Usually, the geometric camera model is obtained from the domain knowledge of the researcher or the camera manufacturer. Often, they choose the simplified model as a trade-off between accuracy and complexity. The model's parameters are usually obtained by solving the constrained optimization problem, given the set of points with known geometry.

2.2 Calibration boards

To achieve a robust calibration, images with repeating patterns are usually used. The camera calibration parameters can be found using prior knowledge of the properties of the pattern, such that the pattern invariants hold on the image. Initially, the chessboard (*OpenCV: Camera Calibration* 2023; V. Douskos, I. Kalisperakis, and G. Karras, 2007) patterns were used (fig. 2.1a).

Later, ArUco (Garrido-Jurado et al., 2014) (fig. 2.1b) and AprilTag (**olsonAprilTagRobustFlexible2011a**) (fig. 2.1d) allowed detecting the orientation of the pattern, as well as uniquely identifying each located pattern even under occlusion. Based on ArUco, ChArUcO (*OpenCV: Camera Calibration* 2023) (fig. 2.1c) was proposed as more robust.

There are also other calibration patterns, some of which are not square (for example, Delitlle (Ha et al., 2017)).

2.3 Camera models

The choice of the camera model depends on the camera's physical properties and the accuracy required. Usually, the parametric models are simpler to use, as they have only a few parameters and deliver good accuracy. The most common are the Double Sphere model (Usenko, Demmel, and Cremers, 2018), the Kannala-Brandt model (Kannala and Brandt, 2006), and the Field-of-View model (Devernay and Faugeras, 2001). In the ill-posed problem of camera calibration, the common choice of the camera model is the division model (Fitzgibbon, 2001). However, Schöps et al., 2020 shows that they tend to have significantly higher errors than the non-parametric (general) models. The Lochman et al., 2021 suggested a framework for converting the parameters of a powerful back-projection Zhang, 2000 model to recover different models' parameters.

(A) Chessboard *OpenCV: Camera Calibration* 2023

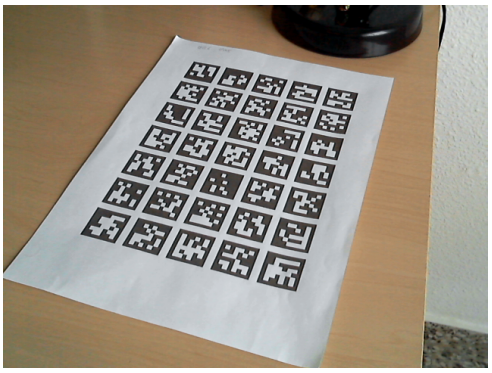

(B) ArUco board *OpenCV: Detection of ArUco Markers* 2023

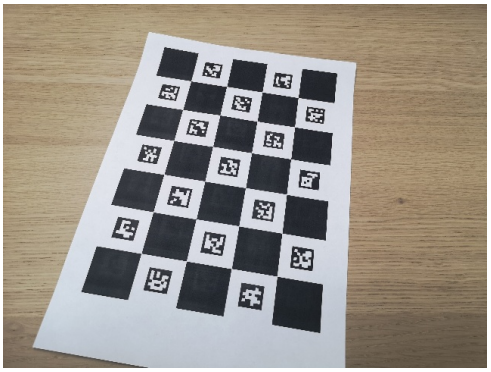

(C) Charuco board *OpenCV: Detection of ChArUco Boards* 2023

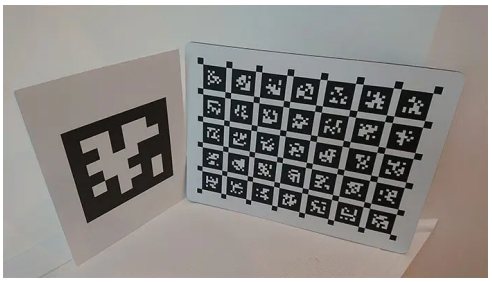

(D) AprilTag board Rosebrock, 2020 (right)

FIGURE 2.1: Calibration boards.

2.4 Camera parameters estimation

Camera calibration using repeating patterns was an important subject for a long time, for example, Schaffalitzky and Zisserman, 1998 in 1998 and Zhang, 2000.

Nevertheless, camera calibration is still an open problem; recently, multiple new approaches have arisen. Davide Scaramuzza, Agostino Martinelli, and Roland Siegwart, 2006 proposed an automatic algorithm for camera calibration, which did not use any model of the specific omnidirectional sensor. Lochman et al., 2021 suggest a universal approach to camera calibration, with a separate step of converting between camera models. Hu et al., 2019 used deep learning to detect ChArUcO boards. Recently, on Oct. 5, 2022, Duisterhof et al., 2022 introduced the iterative approach to camera calibration, which outperforms the previous state-of-the-art approaches for wide-angle cameras.

Add the paper about the feature detection

2.5 Boards' features detection

The detection of the calibration board's features is a crucial step in the camera calibration pipeline. The detection accuracy directly affects the calibration accuracy. Besides the feature detection, it's also important to associate the detected features with the board's corners.

There are various of the feature detection methods. Many of them require prior knowledge of the board's geometry, such as the number of rows and columns, and

require the full visibility of the board. For example, the default OpenCV implementation of the chessboard detection (*OpenCV: Camera Calibration* 2023).

Because of that, other methods were proposed, such as Fuersattel et al., 2016 and Geiger et al., 2012. Those method can detect the board under the partial occlusion and do not require prior knowledge of the board's geometry.

Chapter 3

Background

3.1 Notation

Term	Description
$\mathbf{u} = (u, v, 1)^T$	A point in the board coordinate system
$\mathbf{X} = (X, Y, Z, 1)^T$	A point in the world coordinate system
R	A 3×3 rotation matrix
$\mathbf{t}$	A 3×1 translation vector
α_x	Scale factor in the x direction (pixels/mm)
α_y	Scale factor in the y direction (pixels/mm)
c_x, c_y	Coordinates of the principal point (image center)
θ	Angle between the x and y pixel axes
f	Distance from the camera center to the image plane (focal length)
f_x, f_y	Effective focal lengths in the x and y directions
K	Intrinsic matrix incorporating the scaling, introduced by the focal length
H	A 3×3 matrix viewing $z = 0$ (see section 3.2.5)
λ_n	Distortion coefficients

TABLE 3.1: Notation

3.2 Camera model

In this paper, scene and image points are represented using homogeneous coordinates. This approach allows representing many geometric transformations as linear, which simplifies the mathematical representation of the camera model.

3.2.1 Perspective projection

Should f not be italic?

The perspective projection is a mapping from a 3D point $(X, Y, Z)^T$ in the world coordinate to the 2D coordinate $(u, v)^T$ on the image plane which is distance f from the center of projection. It is given by the perspective projection equation:

$$(u, v)^T = \frac{f}{Z} (X, Y)^T .$$

This equation can be written using the homogeneous coordinates as:

$$\alpha \begin{pmatrix} u \\ v \\ 1 \end{pmatrix} = \begin{bmatrix} f & 0 & 0 & 0 \\ 0 & f & 0 & 0 \\ 0 & 0 & 1 & 0 \end{bmatrix} \begin{pmatrix} X \\ Y \\ Z \\ 1 \end{pmatrix}, \tag{3.1}$$

where $\alpha = 1/Z$ is a scale factor.

3.2.2 Scene to camera projection

A 3D scene point $(X, Y, Z)^T$ can be projected onto the image plane as $R\,(X, Y, Z)^T + \mathbf{t}$, where R is a 3×3 rotation matrix and $\mathbf{t}$ is a 3×1 translation vector. Using the homogeneous coordinates, this can be written as:

$$\begin{bmatrix} R & \mathbf{t} \\ \mathbf{0}^T & 1 \end{bmatrix} \begin{pmatrix} X \\ Y \\ Z \\ 1 \end{pmatrix}. \tag{3.2}$$

3.2.3 Camera to image projection

To project a point from the camera coordinate system to the image plane, we need to apply a homography encoding the camera intrinsic parameters. This is a 3×3 upper-triangular matrix:

$$\begin{bmatrix} \alpha_x & \alpha_x \cot\theta & c_x \\ 0 & \alpha_y \sin\theta & c_y \\ 0 & 0 & 1 \end{bmatrix} \tag{3.3}$$

Is it really upper-triangular?

where:

- α_x and α_y represent the scale factor of the camera in terms of $^{\text{pixels}}/_{\text{mm}}$ in the x and y directions respectively.
- c_x and c_y are the coordinates of the principal point, which is typically the image center.
- $\cot\theta$ and $\sin\theta$ are related to the skew coefficient, which measures the angle between the x and y pixel axes. The variable θ represents this angle.

. For a typical camera, $\theta = \pi/2$ and $\alpha_x = \alpha_y = 1$.

Add reference

Conventionally, the intrinsic matrix incorporates the scaling, introduced by the focal length:

$$K = \begin{bmatrix} \alpha_x f & \alpha_x \cot\theta & c_x \\ 0 & \alpha_y f & c_y \\ 0 & 0 & 1 \end{bmatrix} \begin{bmatrix} f & 0 & 0 \\ 0 & f & 0 \\ 0 & 0 & 1 \end{bmatrix} = \begin{bmatrix} f_x & k & c_x \\ 0 & f_y & c_y \\ 0 & 0 & 1 \end{bmatrix}. \tag{3.4}$$

By incorporating the assumptions into the intrinsic matrix, we can simplify it to:

specify them

$$K = \begin{bmatrix} f & 0 & c_x \\ 0 & f & c_y \\ 0 & 0 & 1 \end{bmatrix}. \tag{3.5}$$

3.2.4 Camera matrix

Add reference

The composition of positioning and orienting the camera, projection, and the imaging transformation can be represented by a 3×4 camera matrix. This matrix can be expressed as:

$$K \begin{bmatrix} I_3 | \mathbf{0} \end{bmatrix} \begin{bmatrix} R & \mathbf{t} \\ \mathbf{0}^T & 1 \end{bmatrix} = K \begin{bmatrix} R | \mathbf{t} \end{bmatrix}, \tag{3.6}$$

Hence, the transformation of a point in the scene by the camera $\mathrm{P}^{3\times4}$ can be formulated as:

$$\alpha (u, v, 1)^T = K \begin{bmatrix} R | \mathbf{t} \end{bmatrix} (X, Y, Z, 1)^T \tag{3.7}$$

with α being $1/Z$.

3.2.5 Projection of the points from the scene plane

When working with the coplanar scene points, we can simplify the projection by assuming that the scene plane is located at $Z = 0$. In this case, the projection of the point becomes:

$$\alpha \begin{pmatrix} u \\ v \\ 1 \end{pmatrix} = K \begin{bmatrix} \mathbf{r_1} & \mathbf{r_2} & \mathbf{r_3} & \mathbf{t} \end{bmatrix} \begin{pmatrix} X \\ Y \\ 0 \\ 1 \end{pmatrix} = K \underbrace{\begin{bmatrix} \mathbf{r_1} & \mathbf{r_2} & \mathbf{t} \end{bmatrix}}_{H} \begin{pmatrix} X \\ Y \\ 1 \end{pmatrix}. \tag{3.8}$$

3.2.6 Distortion

add reference

Specify what's that

The distortion of the image is caused by the lens not being perfectly planar. Typically, the small distoritons caused by lens misalignment are ignored , allowing us to model the distortion as radially symmetric. Then, the function that maps a point $\mathbf{u} = (u, v, 1)^T$ from a retinal plane to the ray direction in the camera coordinate system is given by:

$$g(\mathbf{u}) = (u, v, \psi(r(\mathbf{u})))^T, \tag{3.9}$$

where $r(\mathbf{u}) = \sqrt{u^2 + v^2}$ is the radial distance from the principal point.

Back-projection using the Division Model

Add reference

The division model has a good ability to model the distortion of the wide-angle lenses, and is wildly used . The model is defined as:

$$\psi(r) = 1 + \sum_{n=1}^{N} \lambda_n r^{2n}, \tag{3.10}$$

where λ_n are the distortion coefficients.

Should I explain somewhere how the rays are defined?

The function $\psi(r)$ is not invertible in general. Let $\widehat{\mathbf{X}} = (X, Y, Z)^T = \alpha g(\mathbf{u})$ be a ray in the camera coordinate system.

Then,

$$\frac{\mathbf{X}}{Z} = \left(\tfrac{X}{Z}, \tfrac{Y}{Z}, 1\right)^T \tag{3.11}$$

$$= \left(\frac{\alpha u}{\alpha\psi(r(\mathbf{u}))}, \frac{\alpha v}{\alpha\psi(r(\mathbf{u}))}, 1\right)^T \tag{3.12}$$

$$= \left(\frac{u}{\psi(r(\mathbf{u}))}, \frac{v}{\psi(r(\mathbf{u}))}, 1\right)^T \tag{3.13}$$

From 3.13 we see that

$$\begin{cases} \frac{X}{Z} = \frac{u}{\psi(r(\mathbf{u}))} \\ \frac{Y}{Z} = \frac{v}{\psi(r(\mathbf{u}))} \end{cases} \implies \begin{cases} u = \frac{X\psi(r(\mathbf{u}))}{Z} \\ v = \frac{Y\psi(r(\mathbf{u}))}{Z} \end{cases} \tag{3.14}$$

Now, let $\widehat{r}$ be a root of $r(\mathbf{u}) = \sqrt{\frac{X*\psi(r))^2}{Z} + \frac{Y*\psi(r))^2}{Z}} = r$.
Then, $\mathbf{u} = f(\mathbf{X}) = \frac{\widehat{r}}{r(\mathbf{X})}\mathbf{X}$, where $f(\cdot)$ is the inverse of $g(\cdot)$.

3.2.7 Complete projection and backprojection

Now, the complete projection and backprojection can be formulated as follows:

$$\alpha\mathbf{u} = Kf(H\mathbf{X}) \qquad \text{(Projection)}$$

$$\alpha\mathbf{X} = H^{-1}g(K^{-1}\mathbf{u}) \qquad \text{(Back projection)}$$

.

Chapter 4

Approach

4.1 Feature detection

For the feature detection, we used the approach proposed by Geiger et al., 2012 (see section 2.5 and **??**).

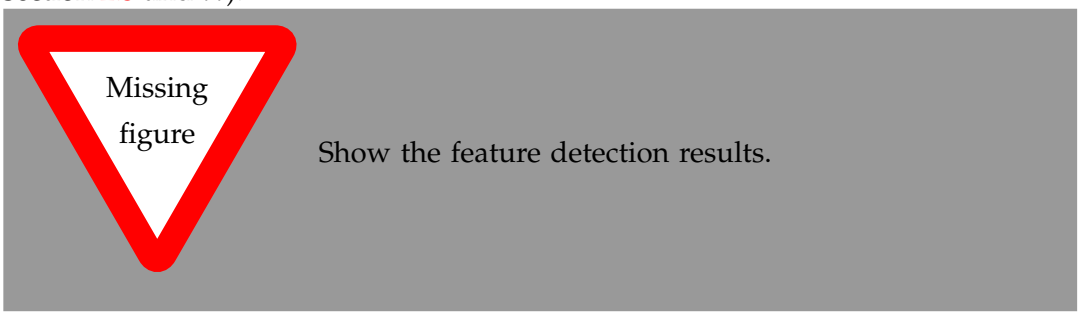

4.2 Camera calibration

In this work, we obtained the camera calibration in two steps: first, we used the approach, proposed by Davide Scaramuzza, Agostino Martinelli, and Roland Siegwart, 2006 to obtain the initial approximation of the camera parameters. Then, we used the optimization to minimize the reprojection error between the board and the back-projected corners.

4.2.1 Reprojection error

The reprojection error is the distance between the reprojected point and the measured one. It is used to evaluate the quality of the camera calibration.

We chose to minimize the reprojection error between the board and back-projected corners, which were initially detected. The projection and back-projection are the inverse of each other, hence minimizing the error between the projection of the board and the detected corners and minimizing the error between the back-projection of the detected corners and the board are equivalent. We minimized the error between the board and the back-projected corners because back-projection does not require the root finding.

Let's define the following variables: $\boldsymbol{\theta} = \left(\theta_x, \theta_y, \theta_z\right)^T$ is the vector of Euler rotation angles, $\mathbf{t} = \left(t_x, t_y, t_z\right)^T$ is the translation vector, $\boldsymbol{\lambda} = \left(\lambda_1, \lambda_2\right)^T$ is the intrinsic parameters vector, is the focal length, and $\mathbf{s} = \left(s_x, s_y\right)^T$ is the sensor size. From the input image, we know the resolution $\mathbf{r} = \left(r_x, r_y\right)^T$. From the rotation vector, we can compute the rotation matrix $\mathbf{R}$ as:

From $\boldsymbol{\theta}$, the rotation matrix R can be calculated as follows:

Doesn't sound very rigorous to me.

Justify why we used 2

Make sure I'm using the correct terms.

$$R = R(\theta_x)R(\theta_y)R(\theta_z) \tag{4.1}$$

Is the notation ok?

where

$$R(\theta_x) = \begin{bmatrix} 1 & 0 & 0 \\ 0 & \cos(\theta_x) & -\sin(\theta_x) \\ 0 & \sin(\theta_x) & \cos(\theta_x) \end{bmatrix} \tag{4.2}$$

$$R(\theta_y) = \begin{bmatrix} \cos(\theta_y) & 0 & \sin(\theta_y) \\ 0 & 1 & 0 \\ -\sin(\theta_y) & 0 & \cos(\theta_y) \end{bmatrix} \tag{4.3}$$

$$R(\theta_z) = \begin{bmatrix} \cos(\theta_z) & -\sin(\theta_z) & 0 \\ \sin(\theta_z) & \cos(\theta_z) & 0 \\ 0 & 0 & 1 \end{bmatrix} \tag{4.4}$$

Then, H is given by:

$$H = \begin{bmatrix} \mathbf{r_1} & \mathbf{r_2} & \mathbf{t} \end{bmatrix}. \tag{4.5}$$

We can compute the intrinsic camera matrices as follows:

$$K = \begin{pmatrix} \frac{fr_x}{s_x} & 0 & \frac{r_x}{2} \\ 0 & \frac{fr_y}{s_y} & \frac{r_y}{2} \\ 0 & 0 & 1 \end{pmatrix}, \tag{4.6}$$

.

Then, the back-projection of a 2D point $\mathbf{u} = (u, v, 1)$ into a scene point with $Z = 0$ $\mathbf{X} = (X, Y, 1)$ is given by:

$$\mathbf{X} = Hg_{\lambda_1,\lambda_2}(K^{-1}\mathbf{u}). \tag{4.7}$$

4.2.2 Initial approximation

Davide Scaramuzza, Agostino Martinelli, and Roland Siegwart, 2006 proposed an automatic method for camera calibration, which consisted of the following steps:

- Solving for the camera extrinsic parameters
- Solving for the camera intrinsic parameters
- Linear refinement of the intrinsic and extrinsic parameters
- Iterative center detection
- Non-linear refinement

In this work, we focused on the single image, while the original approach relied on the multiple images. Therefore, we used only the first two steps of the algorithm.

Solving for the camera extrinsic parameters

To derive the solver for the camera extrinsic parameters, start from eq. (Projection):

$$\alpha \mathbf{u} = Kf(H\mathbf{X}) \tag{4.8}$$

$$\alpha K^{-1}\mathbf{u} = f(H\mathbf{X}) \qquad \text{Move } K \text{ to the left side} \tag{4.9}$$

$$\alpha g(K^{-1}\mathbf{u}) = g(f(H\mathbf{X})) \qquad \text{Set } \widehat{\mathbf{u}} = K^{-1}\mathbf{u}\text{; apply } g(\cdot) \text{ to both sides} \tag{4.10}$$

$$\alpha \begin{pmatrix} \widehat{u}_x \\ \widehat{u}_y \\ \psi(r(\widehat{\mathbf{u}})) \end{pmatrix}^T = H\mathbf{X} \tag{4.11}$$

$$\tag{4.12}$$

For K we used the placeholder values. f was set to a constant value for the typical consumer camera, and c_x, c_y were set to the center of the image. The correct values will be computed during the optimization section 4.2.3.

To eliminate the dependency on the scale α, multiply both sides vectorially by $g(\widehat{\mathbf{u}})$:

$$\alpha g(\widehat{\mathbf{u}}) \times g(\widehat{\mathbf{u}}) = g(\widehat{\mathbf{u}}) \times H\mathbf{X} = 0 \implies \left(\widehat{u}, \widehat{v}, \psi(r(\widehat{\mathbf{u}}))\right)^T \times \begin{bmatrix} \mathbf{r_1} & \mathbf{r_2} & \mathbf{t} \end{bmatrix}^T \mathbf{X} = 0 \tag{4.13}$$

.

From eq. (4.13), we can see that a point contributes to three homogeneous equations:

$$\widehat{v}(t_1X + t_2Y + t_3) - g(r(\widehat{\mathbf{u}}))(r_{12}X + r_{22}Y + t_2) = 0 \tag{4.14}$$

$$g(r(\widehat{\mathbf{u}}))(r_{11}X + r_{12}Y + t_1) - \widehat{u}(t_1X + t_2Y + t_3) = 0 \tag{4.15}$$

$$\widehat{u}(r_{12}X + r_{22}Y + t_2) - \widehat{v}(r_{11}X + r_{12}Y + t_1) = 0 \tag{4.16}$$

Only eq. (4.16) is linear in the unknowns. Each point gives a single equation. Now, by rewriting the equation in the matrix form $M \cdot H = 0$, where $H = \left(r_{11}, r_{12}, r_{12}, r_{22}, t_1, t_2\right)$ we get:

$$M = \begin{bmatrix} -\widehat{v}_1X_1 & -\widehat{v}_1Y_1 & -\widehat{u}_1X_1 & -\widehat{u}_1Y_1 & -\widehat{v}_1 & -\widehat{u}_1 \\ \vdots & \vdots & \vdots & \vdots & \vdots & \vdots \\ -\widehat{v}_NX_N & -\widehat{v}_NY_N & -\widehat{u}_NX_N & -\widehat{u}_NY_N & -\widehat{v}_N & -\widehat{u}_N \end{bmatrix} \tag{4.17}$$

, where N is the number of points.

The linear estimate of H is found by minimizing $\|M \cdot H\|^2$ using SVD. The solution is known up to a scale factor.

To find t_1 and t_2, note that $\mathbf{r_1}$ and $\mathbf{r_2}$ are orthonormal:

$$\begin{cases} \lambda^2 r_{11}r_{12} + \lambda^2 r_{12}r_{22} + \lambda^2 t_1 t_2 = 0 & \text{(4.18a)} \\ \lambda\sqrt{r_{11}^2 + r_{12}^2 + t_1^2} = 1 & \text{(4.18b)} \\ \lambda\sqrt{r_{12}^2 + r_{22}^2 + t_2^2} = 1 & \text{(4.18c)} \end{cases}$$

, where λ is non-zero multiplier.

Now, to solve for t_1 and t_2, first find possible values for t_2^2:

$$-\frac{r_{11}r_{12}+r_{12}r_{22}}{t_2} = t_1 \quad \text{Solve eq. (4.18a) for } t_1 \tag{4.19}$$

$$\sqrt{\lambda^2\left(\frac{(r_{11}r_{12}+r_{12}r_{22})^2}{t_2^2}+r_{11}^2+r_{12}^2\right)} = 1 \quad \text{Substitute into eq. (4.18b)} \tag{4.20}$$

$$\lambda^2\left(\frac{(r_{11}r_{12}+r_{12}r_{22})^2}{t_2^2}+r_{11}^2+r_{12}^2\right) = 1 \quad \text{Square both sides} \tag{4.21}$$

$$\lambda^2\left(\frac{(r_{11}r_{12}+r_{12}r_{22})^2}{t_2^2}+r_{11}^2+r_{12}^2-r_{12}^2-r_{22}^2-t_2^2\right) = 0 \quad \text{Subtract eq. (4.18c)} \tag{4.22}$$

$$\frac{(r_{11}r_{12}+r_{12}r_{22})^2}{t_2^2}+r_{11}^2+r_{12}^2-r_{12}^2-r_{22}^2-t_2^2 = 0 \quad \text{Divide both by } \lambda^2 \tag{4.23}$$

$$t_2^4-(r_{11}^2+r_{12}^2-r_{12}^2-r_{22}^2)t_2^2-(r_{11}r_{12}+r_{12}r_{22})^2 = 0 \quad \text{Multiply by } t_2^2 \tag{4.24}$$

$$t_2^4-(r_{11}^2+r_{12}^2-r_{12}^2-r_{22}^2)t_2^2-(r_{11}r_{12}+r_{12}r_{22})^2 = 0 \tag{4.25}$$

Now, solve eq. (4.25) for t_2^2, and take a root to find possible values for t_2.

To find t_1, substitute the found values for t_2 into eq. (4.19) or eq. (4.23) depending on the value of t_2:

$$\begin{cases} t_1 = -\dfrac{r_{11}r_{12}+r_{12}r_{22}}{t_2} & t_2 \neq 0 \quad (4.26a) \\ t_1 = r_{11}^2+r_{12}^2-r_{12}^2-r_{22}^2 & t_2 = 0 \quad (4.26b) \end{cases}$$

Now, it's possible to find H for each of the pairs of t_1 and t_2.

Lastly, to select the correct H, the author assumes that one of the boards' corners has the coordinates $(0,0)^T$. Then, the rotation wouldn't affect this point, and it would be projected to $(t_1,t_2)^T$. Hence, the best matrix would be such that has the closest $(t_1,t_2)^T$ to $(X,Y)^T$ of the corner, which is associated with the board's corner with corrdinates $(0,0)^T$.

However, often the algorithm finds who matrices H such that they have the same t_1 and t_2, but different r_{11}, r_{12}, r_{21}. To find the best matrix, we found the intrinsic values for each of them, and backprojected the board's corners using both matrices. Then, we used the one which gave the smallest reprojection error.

Solving for the camera intrinsic parameters

Now, to find the rest of the parameters, we substitute the values, found in the previous step into eq. (4.14) and eq. (4.15). We assumed the number of the division model's parameter to be equal to 2, and the scalar multiplier to be equal to 1 section 3.2.6:

$$\begin{bmatrix} A_1\rho_1^2 & A_1\rho_1^4 & -v_1 \\ C_1\rho_1^2 & C_1\rho_1^4 & -v_1 \\ \cdots & \cdots & \cdots \\ A_N\rho_N^2 & A_N\rho_N^4 & -v_N \\ C_N\rho_N^2 & C_N\rho_N^4 & -v_N \end{bmatrix} \cdot \begin{bmatrix} \lambda_1 \\ \lambda_2 \\ t_3 \end{bmatrix} = \begin{bmatrix} B_1-A_1 \\ D_1-C_1 \\ \cdots \\ B_N-A_N \\ D_N-C_N \end{bmatrix} \tag{4.27}$$

, where

$$A_i = r_{21}X_i + r_{22}Y_i + t_2 \tag{4.28}$$
$$B_i = v_i(r_{31}X_i + r_{32}Y_i) \tag{4.29}$$
$$C_i = r_{11}X_i + r_{12}Y_i + t_1 \tag{4.30}$$
$$D_i = u_i(r_{31}X_i + r_{32}Y_i) \tag{4.31}$$
$$\tag{4.32}$$

The solution can be found using the least squares method.

4.2.3 Optimization

The loss function is the sum of the squared reprojection errors between the board and the back-projected corners, which were initially detected:

$$L = \sum_{i=1}^{N} \left\| Hg_{\lambda_1,\lambda_2}(K^{-1}\mathbf{u_i}) - \mathbf{X_i} \right\|^2. \tag{4.33}$$

For the initial guess, we used the randomly chosen constant small values.

The model converged to the same results compared to the initial parameters, set using the Scaramuzza solver, unless the initial guess was very degenerate (i.e. R was such that the board plane passed through the principal point, and all backprojected points were projected onto the same line).

This issue also occured with random small initial values, due to the best approximation for R which minimizes L when the distance from the back-projected board from the measure one was high (i.e., the t was far from the true value) being the degenerate solution. In order to avoid this issue, we first optimized only the t, until the loss function converged, meaning that t is close to the true value.

Am I using the term correctly?

However, another issue was that when the board was rotated close to the 180°, R once again converged to the degenerate solution. In order to avoid this issue, we found the solution with initial θ_z set to value, close to 0° and 180°, and then used the solution which minimized the loss function.

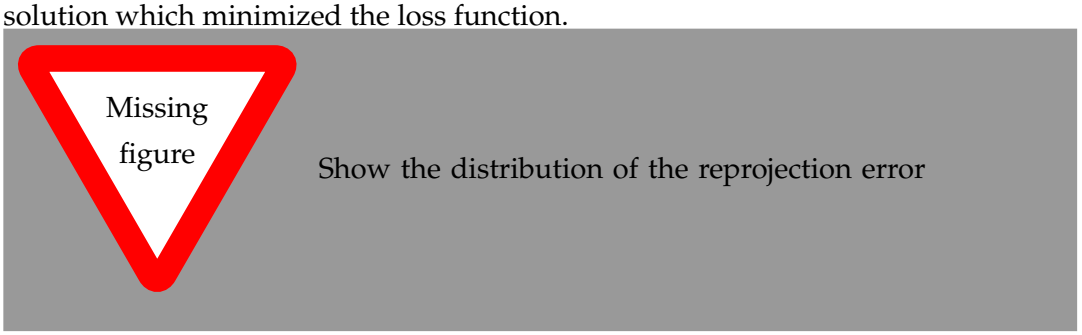

.

4.3 Additional features detection

Add ref to the figure

Often, not all of the board's corners were detected initially. Firstly, we assumed that the whole board was detected, and imputed the missing points in the board space.. Then, we tried extending the board points.

Show the image, the respective board, and the imputed points

We used the obtained camera parameters to then project the imputed board points into the image space.

4.4 Classifier

In this work, we used the method, proposed by Geiger et al., 2012 as it didn't require the whole board to be visible, automatically determines the board's number of rows and columns and worked quite well on highly-distorted images.

In this work, we directly used the following steps from the algorithm:

1. Corner detection
2. Sub-pixel corner and orientation refinement

4.4.1 Corner detection

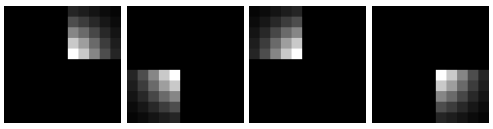

(A) Corner prototype 1 (A, B, C, D)

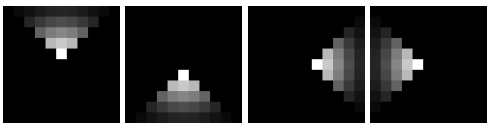

(B) Corner prototype 2 (A, B, C, D)

FIGURE 4.1: Corner prototypes (Geiger et al., 2012)

According to Geiger et al., 2012, the following approach proved to be more robust to image clutter and blur than other common choices (Harris and Stephens, 1988; Shi and Tomasi, 2000).

To detect corners in a grayscale image I, the author used two $n \times n$ prototypes for axis-aligned and 45° rotated corners, respectively. Each prototype is constructed using four filter kernels $\{A, B, C, D\}$ (fig. 4.1). The corner likelihood c at each pixel is computed by:

$$\begin{aligned} c &= \max\left(s_1^1, s_2^1, s_1^2, s_2^2\right) \\ s_1^i &= \min\left(\min\left(f_A^i, f_B^i\right) - \mu, \mu - \min\left(f_C^i, f_D^i\right)\right) \\ s_2^i &= \min\left(\mu - \min\left(f_A^i, f_B^i\right), \min\left(f_C^i, f_D^i\right) - \mu\right) \\ \mu &= 0.25\left(f_A^i + f_B^i + f_C^i + f_D^i\right) \end{aligned} \tag{4.34}$$

Then, the authors apply the conservative non-maximum suppression to the response map, and additionally filter the corners by assuring that there are two modes of the gradient directions.

4.4.2 Sub-pixel Corner and Orientation Refinement

Sub-pixel accurate corner locations and edge orientations are refined using the following optimizations:

For sub-pixel corner localization, the corner $\mathbf{c}$ in a 2D space $\mathbb{R}^2$ is refined using the assumption that the gradient direction $\mathbf{g_p}$ at each pixel $\mathbf{p}$ in the small neighbourhood around the corner is orthogonal to $\mathbf{p} - \mathbf{c}$.

$$\mathbf{c} = \arg\min_{\mathbf{c}'} \sum_{\mathbf{p} \in \mathcal{N}_\mathbf{I}(\mathbf{c}')} \left(\mathbf{g}_\mathbf{p}^T \left(\mathbf{p} - \mathbf{c}' \right) \right)^2 \tag{4.35}$$

For the orientation refinement, authors minimize the distance from the orientation vectors $\mathbf{e_1}, \mathbf{e_2}$ to the gradient directions $\mathbf{g_p}$ in the neighbourhood of the corner.

$$\mathbf{e}_i = \arg\min_{\mathbf{e}_i'} \sum_{\mathbf{p} \in \mathcal{M}_i} \left(\mathbf{g}_\mathbf{p}^T \mathbf{e}_i' \right)^2 \quad \text{s.t. } \mathbf{e}_i'^T \mathbf{e}_i' = 1 \tag{4.36}$$

.

The original paper then used a number of checks to further prune the detected corners, and extending line by line the initial board, formed from the random close points which made a square . We did not require that, since we already had the board, and we directly used the response map to find the corners.

Make sure that's accurate, and reference. Also, the sentence is too compicated

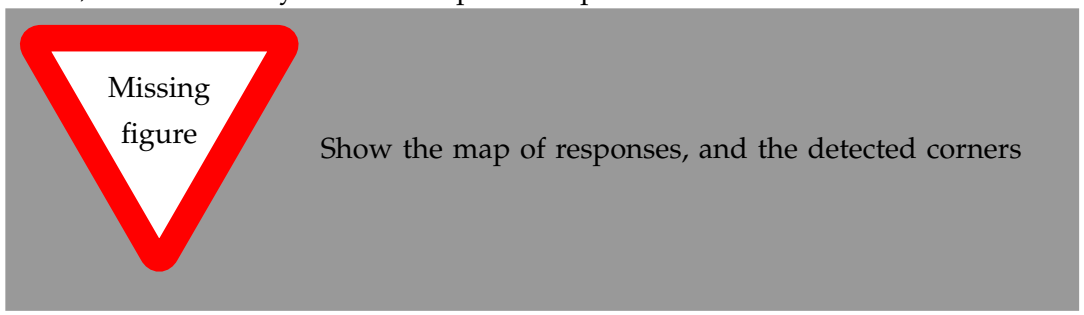

To create a training dataset, we collected the true and false positives from the corners we already had:

For each of the detected corners on all images, we collected the values of the response function at the previously detected corners, and around them. We didn't collect the values of all of the pixels, because then we would have got too optimistic values for selecting the true positives.

Rephrase

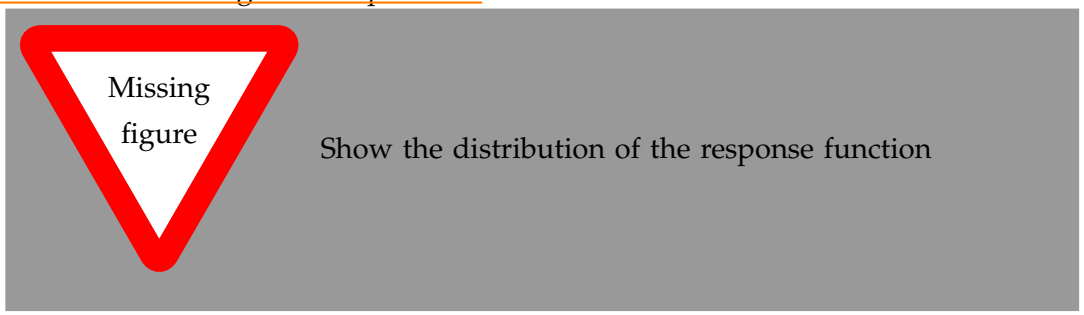

We trained a binary classifier, using the collected data, and then used it to detect the true corners.

Chapter 5

Experiments

5.1 Simulator

We created a symulator to generate distorted points. We used it to test the solver, and test the correctness of projection and back-projection points.

5.2 Metrics

- Reprojection error
- Number of detected corners

5.3 Dataset

For the project, we need highly distorted photos of calibration boards. It takes a lot of work to generate such a dataset, as cameras which produce such images are usually expensive. Therefore, it would be preferable to use an existing dataset.

Lochman et al. (2021) collected a wide number of datasets, typically used in the field for the benchmarking of the camera calibration. They're provided in a Deltille *Deltille Detector* 2023 format, and are well documented:

Kalibr contains several established datasets that are commonly used for testing the accuracy of camera calibration frameworks: Double Sphere Usenko, Demmel, and Cremers, 2018, EuRoC Burri et al., 2016, TUM VI Schubert et al., 2018, and ENTANIYA 1 *Calibration of a 250deg Fisheye Lens ů Issue #242 ů Ethz-Asl/Kalibr* 2023. The Kalibr calibration framework was used in the original publications cited above, hence the name of the dataset. As a calibration pattern, AprilGrid with 6x6 tags of 88 mm size was used. In total, the datasets contain approximately 800 images.

OCamCalib D. Scaramuzza, A. Martinelli, and R. Siegwart, 2006 is a dataset of approximately 300 images. As a calibration pattern, the checkerboard pattern of different sizes was used.

UZH *Are We Ready for Autonomous Drone Racing? The UZH-FPV Drone Racing Dataset | Request PDF* 2023 is a dataset of approximately 800 images collected using the following cameras: As a calibration pattern, AprilGrid with 4x5 tags of 75 mm size was used. The dataset contains approximately 800 images.

OV Duisterhof et al., 2022 is a dataset of approximately 1400 images. It was collected using eight stereo cameras. As a calibration pattern, the checkerboard pattern with 9x6 tags of 22 mm size was used.

Duisterhof et al. (2022) also provide their dataset from the TartanCalib project, but it is quite challenging to use it as it comes in the Robot Operating System (ROS) .bag format.

Probably, remove everything but BabelCalib, as

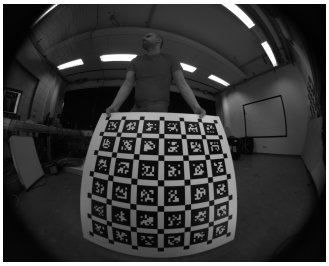

(A) Kalibr

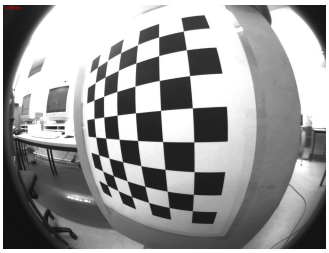

(B) OCamCalib

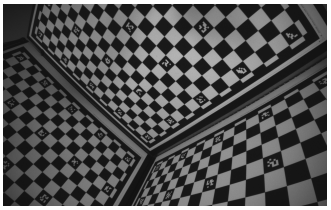

(C) OV

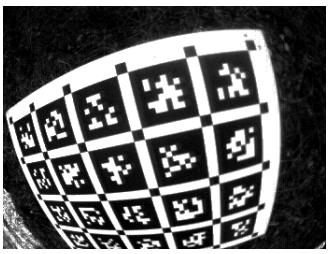

(D) UZH

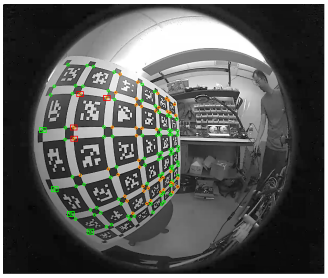

(E) TartanCalib

FIGURE 5.1: Images from the datasets

Chapter 6

Conclusions

Bibliography

Are We Ready for Autonomous Drone Racing? The UZH-FPV Drone Racing Dataset | Request PDF (2023). URL: https://www.researchgate.net/publication/335144528_Are_We_Ready_for_Autonomous_Drone_Racing_The_UZH-FPV_Drone_Racing_Dataset (visited on 01/30/2023).

Burri, Michael et al. (Jan. 25, 2016). "The EuRoC Micro Aerial Vehicle Datasets". In: *The International Journal of Robotics Research* 35. DOI: 10.1177/0278364915620033.

Calibration of a 250deg Fisheye Lens ů Issue #242 ů Ethz-Asl/Kalibr (2023). GitHub. URL: https://github.com/ethz-asl/kalibr/issues/242 (visited on 01/30/2023).

Deltille Detector (Jan. 28, 2023). Meta Archive. URL: https://github.com/facebookarchive/deltille (visited on 01/30/2023).

Devernay, Frédéric and Olivier Faugeras (Aug. 1, 2001). "Straight Lines Have to Be Straight". In: *Machine Vision and Applications* 13.1, pp. 14–24. ISSN: 1432-1769. DOI: 10.1007/PL00013269. URL: https://doi.org/10.1007/PL00013269 (visited on 01/15/2023).

Duisterhof, Bardienus P. et al. (Oct. 5, 2022). *TartanCalib: Iterative Wide-Angle Lens Calibration Using Adaptive SubPixel Refinement of AprilTags*. DOI: 10.48550/arXiv.2210.02511. arXiv: 2210.02511 [cs]. URL: http://arxiv.org/abs/2210.02511 (visited on 01/05/2023). preprint.

Fitzgibbon, A.W. (Dec. 2001). "Simultaneous Linear Estimation of Multiple View Geometry and Lens Distortion". In: *Proceedings of the 2001 IEEE Computer Society Conference on Computer Vision and Pattern Recognition. CVPR 2001*. Proceedings of the 2001 IEEE Computer Society Conference on Computer Vision and Pattern Recognition. CVPR 2001. Vol. 1, pp. I–I. DOI: 10.1109/CVPR.2001.990465.

Fuersattel, Peter et al. (Mar. 1, 2016). "OCPAD Occluded Checkerboard Pattern Detector". In: pp. 1–9. DOI: 10.1109/WACV.2016.7477565.

Garrido-Jurado, S. et al. (June 1, 2014). "Automatic Generation and Detection of Highly Reliable Fiducial Markers under Occlusion". In: *Pattern Recognition* 47.6, pp. 2280–2292. ISSN: 0031-3203. DOI: 10.1016/j.patcog.2014.01.005. URL: https://www.sciencedirect.com/science/article/pii/S0031320314000235 (visited on 01/05/2023).

Geiger, Andreas et al. (May 2012). "Automatic Camera and Range Sensor Calibration Using a Single Shot". In: *2012 IEEE International Conference on Robotics and Automation*. 2012 IEEE International Conference on Robotics and Automation, pp. 3936–3943. DOI: 10.1109/ICRA.2012.6224570.

Ha, Hyowon et al. (Oct. 1, 2017). "Deltille Grids for Geometric Camera Calibration". In: pp. 5354–5362. DOI: 10.1109/ICCV.2017.571.

Harris, C. and M. Stephens (1988). "A Combined Corner and Edge Detector". In: *Procedings of the Alvey Vision Conference 1988*. Alvey Vision Conference 1988. Manchester: Alvey Vision Club, pp. 23.1–23.6. DOI: 10.5244/C.2.23. URL: http://www.bmva.org/bmvc/1988/avc-88-023.html (visited on 05/27/2023).

Hu, Danying et al. (July 1, 2019). *Deep ChArUco: Dark ChArUco Marker Pose Estimation*. DOI: 10.48550/arXiv.1812.03247. arXiv: 1812.03247 [cs]. URL: http://arxiv.org/abs/1812.03247 (visited on 01/05/2023). preprint.

Kannala, Juho and Sami Brandt (Sept. 1, 2006). "A Generic Camera Model and Calibration Method for Conventional, Wide-Angle, and Fish-Eye Lenses". In: *IEEE transactions on pattern analysis and machine intelligence* 28, pp. 1335–40. DOI: 10.1109/TPAMI.2006.153.

Krogius, Maximilian, Acshi Haggenmiller, and Edwin Olson (Nov. 2019). "Flexible Layouts for Fiducial Tags". In: *2019 IEEE/RSJ International Conference on Intelligent Robots and Systems (IROS)*. 2019 IEEE/RSJ International Conference on Intelligent Robots and Systems (IROS), pp. 1898–1903. DOI: 10.1109/IROS40897.2019.8967787.

Lochman, Yaroslava et al. (Oct. 28, 2021). *BabelCalib: A Universal Approach to Calibrating Central Cameras*. DOI: 10.48550/arXiv.2109.09704. arXiv: 2109.09704 [cs]. URL: http://arxiv.org/abs/2109.09704 (visited on 01/05/2023). preprint.

OpenCV: Camera Calibration (2023). URL: https://docs.opencv.org/4.x/dc/dbb/tutorial_py_calibration.html (visited on 01/15/2023).

OpenCV: Detection of ArUco Markers (2023). URL: https://docs.opencv.org/4.x/d5/dae/tutorial_aruco_detection.html (visited on 01/15/2023).

OpenCV: Detection of ChArUco Boards (2023). URL: https://docs.opencv.org/3.4/df/d4a/tutorial_charuco_detection.html (visited on 01/30/2023).

Rosebrock, Adrian (Nov. 2, 2020). *AprilTag with Python*. PyImageSearch. URL: https://pyimagesearch.com/2020/11/02/apriltag-with-python/ (visited on 01/30/2023).

Scaramuzza, D., A. Martinelli, and R. Siegwart (2006). "A Flexible Technique for Accurate Omnidirectional Camera Calibration and Structure from Motion". In: *Fourth IEEE International Conference on Computer Vision Systems (ICVS'06)*, pp. 45–45. DOI: 10.1109/ICVS.2006.3. URL: http://ieeexplore.ieee.org/document/1578733/ (visited on 01/30/2023).

Scaramuzza, Davide, Agostino Martinelli, and Roland Siegwart (Oct. 1, 2006). "A Toolbox for Easily Calibrating Omnidirectional Cameras". In: IEEE International Conference on Intelligent Robots and Systems. DOI: 10.1109/IROS.2006.282372.

Schaffalitzky, Frederik and Andrew Zisserman (Sept. 18, 1998). "Geometric Grouping of Repeated Elements within Images". In: *In Shape, Contour and Grouping in Computer Vision LNCS* 1681. ISSN: 978-3-540-66722-3. DOI: 10.5244/C.12.2.

Schöps, Thomas et al. (June 23, 2020). *Why Having 10,000 Parameters in Your Camera Model Is Better Than Twelve*. DOI: 10.48550/arXiv.1912.02908. arXiv: 1912.02908 [cs]. URL: http://arxiv.org/abs/1912.02908 (visited on 01/05/2023). preprint.

Schubert, David et al. (Oct. 1, 2018). *The TUM VI Benchmark for Evaluating Visual-Inertial Odometry*, p. 1687. 1680 pp. DOI: 10.1109/IROS.2018.8593419.

Shi, Jianbo and Carlo Tomasi (Mar. 3, 2000). "Good Features to Track". In: *Proceedings / CVPR, IEEE Computer Society Conference on Computer Vision and Pattern Recognition. IEEE Computer Society Conference on Computer Vision and Pattern Recognition* 600. DOI: 10.1109/CVPR.1994.323794.

Usenko, Vladyslav, Nikolaus Demmel, and Daniel Cremers (July 24, 2018). *The Double Sphere Camera Model*.

V. Douskos, I. Kalisperakis, and G. Karras (2007). "Automatic Calibration of Digital Cameras Using Planar Chessboard Patterns". In.

Zhang, Z. (Nov. 2000). "A Flexible New Technique for Camera Calibration". In: *IEEE Transactions on Pattern Analysis and Machine Intelligence* 22.11, pp. 1330–1334. ISSN: 1939-3539. DOI: 10.1109/34.888718.